Available online at www.sciencedirect.com

SciVerse ScienceDirect

Ceramics International 39 (2013) 3001–3006

CERAMICS INTERNATIONAL

www.elsevier.com/locate/ceramint

Pore structure dependence with the sintering time for dense ceramic bulk $YBa_2Cu_3O_y$

J.L. Gonzalez[a,*], C.K. Piumbini[a], W.L. Scopel[a,c], F. Deleprani[a], A. Gomes[b], A. Cunha[a]

[a] Universidade Federal do Espírito Santo, Vitória, ES 29075 910, Brazil
[b] Universidade Federal do Rio de Janeiro, Rio de Janeiro, RJ 21494 901, Brazil
[c] Universidade Federal Fluminense, Volta Redonda, RJ 27255 125, Brazil

Received 20 August 2012; received in revised form 23 September 2012; accepted 23 September 2012
Available online 28 September 2012

Abstract

Technological applications of bulk high-T_C superconductors, in particular of $YBa_2Cu_3O_y$, require polycrystalline materials with improved physical properties which strongly depend on the presence of pores and their characteristics. In this work we have studied the pore structure and their principal features in dense $YBa_2Cu_3O_y$ samples prepared with different sintered times. The samples were prepared through a classic solid state reaction method. The critical temperatures of the samples were measured by using zero field cooling magnetization. The pore structure and their features were studied through N_2 sorption measurements. Our experimental results show that the principal characteristics of the pore structure depend on the sintering time. In particular, samples sintered during 24 h show a higher porosity and external surface area, as also a more heterogeneous pore distribution slightly shifted to the low pore widths region, when compared to other samples sintered by using different times. Our work shows the importance of the sintering conditions regarding the controlling of the porous character of bulk YBCO superconductors.

Keywords: C. Superconductivity; D. Oxide superconductors; B. Porosity; A. Sintering

1. Introduction

Bulk superconductors with high critical temperatures (HTSC) have shown a great range of technological potentialities, like for example resistive and inductive fault current limiters [1], laboratory magnets [2], brushless synchronous motors [3], low-loss magnetic bearings used in efficient energy-storage flywheel devices [4], beside others [5]. These advances have been possible, in part, due to a better understanding of the physical properties of the YBCO123 system which has been largely recognized as the most important HTSC for technological applications.

The development of practical superconductors needs compact materials with improved superconducting and mechanical properties, where one important requirement is a controlled porosity of the samples. In fact, the presence of pores strongly affects, or modify in different ways, the superconducting and mechanical properties of YBCO123 samples [6,7]. Pores can be filled by different liquid components resulting in secondary phases, and also several mechanical properties, like hardness, strength and toughness are strongly dependent on the porosity level [8]. From the superconducting point of view, important properties like the magnetic field trapped inside the superconductor, the critical current density, and also the chemical reactivity (in particular oxygen absorption) are tightly influenced by the presence of pores [9].

Several techniques and methods used in the fabrication of polycrystalline YBCO123 samples have shown some possibilities to controlling the porosity. Modern melt-texturing methods, like for example top-seeded melt-growth and liquid infiltration growth represent attempts to produce single-domain bulk YBCO aided by the presence of the liquid phase [10,11], reporting a healing of pores in Y123/Y211 composites, as also a decreasing in porosity [12,13]. Other attempts to control the pores quantity have been performed

*Corresponding author at: Universidade Federal de Espírito Santo. Av. Fernando Ferrari, 514, Goiabeiras, Vitória, ES, CEP 29075-910, Brasil.
E-mail address: jlga.1966@gmail.com (J.L. Gonzalez).

0272-8842/$ - see front matter © 2012 Elsevier Ltd and Techna Group S.r.l. All rights reserved.
http://dx.doi.org/10.1016/j.ceramint.2012.09.078

through the addition of silver in bulk samples [14,15], which has shown, for example, that the hardness can be less sensitive to the porosity level [16]. On the other hand, high density YBCO123 samples can be easily produced by the solid-state traditional method by increasing the sintering temperatures. Indeed, some studies have shown that samples with optimal densities can be obtained by sintering at around 950 °C [17–19], which is below the peritectic melting temperature of the 123 compound in air [20]. Nevertheless, for these samples one point which has not been deeply discussed is how the sintering time can modify the presence of pores and their principal features.

The nitrogen adsorption/desorption is a powerful technique that has been used to determine many of the characteristics of the pores inside different samples [21], once it can detect a porosity level which is undetectable through the use of scanning electron microscope. From these measurements key physical features of the pore structure, like specific surface area, total pore volume, average pore size and pore distribution can be experimentally investigated [22]. It is also important to note that N_2 sorption measurements are performed at 77 K, which is the operation temperature for many applications of YBCO123. In this work we have sintered YBCO123 samples at 950 °C but with different times by using the solid-state reaction method. In order to explore how the sintering time affects the pore structure of YBCO123 samples, we have used the N_2 adsorption/desorption measurements. Our experimental results confirm the superconducting character of all the produced samples, and also that the use of different times influences the principal features of the pores. In particular, the porosity level and the external surface area of the particles are maxima for sintering time around 24 h. Also for this sample (sintered with 24 h) is verified a significant generation of micropores, the pore distribution is shifted to the low widths region (consequently the average pore size is lower), and finally, the pore distribution seems to be more heretogeneous.

2. Experimental

$YBa_2Cu_3O_{7-y}$ samples were prepared by a solid state reaction method as described elsewhere. Initially, pure powders (99.99%) of Y_2O_3, $BaCO_3$ and CuO were dried, milled (2 h) and weighted in appropriate stoichiometric proportions. Latter, two calcination processes were performed on the powders at a temperature of about 850 °C (24 h) with an increase (decrease) rate of 300 °C/h. After that, the pre-formed samples were sintered at a temperature of 950 °C but with different sintering times, specifically, 6 h, 12 h, 24 h, 48 h and 72 h (identified through the work as 6 h, 12 h, 24 h, 48 h and 72 h sample, respectively). The increase rate during the sintering was the same one as used before, i.e., 300 °C/h, however all the samples were quenched in air from the sintering temperature at the different times specified above. Finally an annealing in partial O_2 pressure was performed at 450 °C and during 5 h for all the samples. Reground of the powders was performed between the different stages of the process.

The superconducting properties of YBCO(1 2 3) samples are strongly affected by the sintering conditions. It has been shown that the control of the atmospheres can modify the melting point of YBCO(1 2 3) [23] leading to different sintering routes. This can modify in different ways the intergranular and intragranular properties of the samples and in particular it has a strong influence on the morphology and nature of the grain boundaries in the samples [24,25]. Thus, it should be stressed that our results reported herein are particular for our sintering conditions, i.e., YBCO(1 2 3) samples quenched in air.

In order to determine the critical temperatures of the ceramic samples, magnetization measurements in ZFC condition were performed through a PPMS system from the *Quantum Design*. Finally the samples were reground, and N_2 adsorption/desorption measurements in the range of relative pressures from $\sim 10^{-6}$ to 0.99 were performed on the powders by using an equipment *Autosorb−1* from the *Quantachrome* instruments. The measurements were performed at nitrogen liquid temperature with nitrogen gas as adsorbate. All the powders were outgassed at 200 °C for 15 h before the measurements.

3. Results and discussion

As a first point, magnetization measurements as a function of the temperature and in zero field cooling conditions were performed to verify the superconducting character of the samples. For all the samples a magnetic field of 50 Oe was applied at 10 K and later the magnetic moment was measured for temperatures between 10 K and 100 K. No corrections for the demagnetization fields were used in the measurements since the principal goal was to find the critical temperature of the samples. In Fig. 1 it can be observed the presence of a superconducting transition in all the samples. The critical temperatures were taken at the onset of the diamagnetic signals and this can be better observed in the inset of the figure, which shows

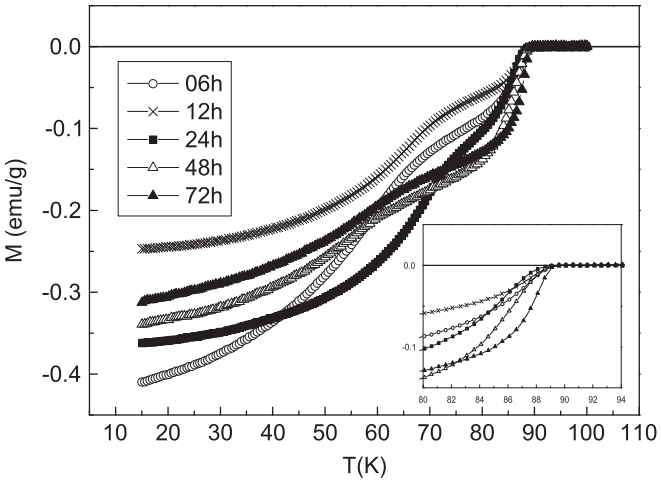

Fig. 1. Magnetization as a function of the temperature.

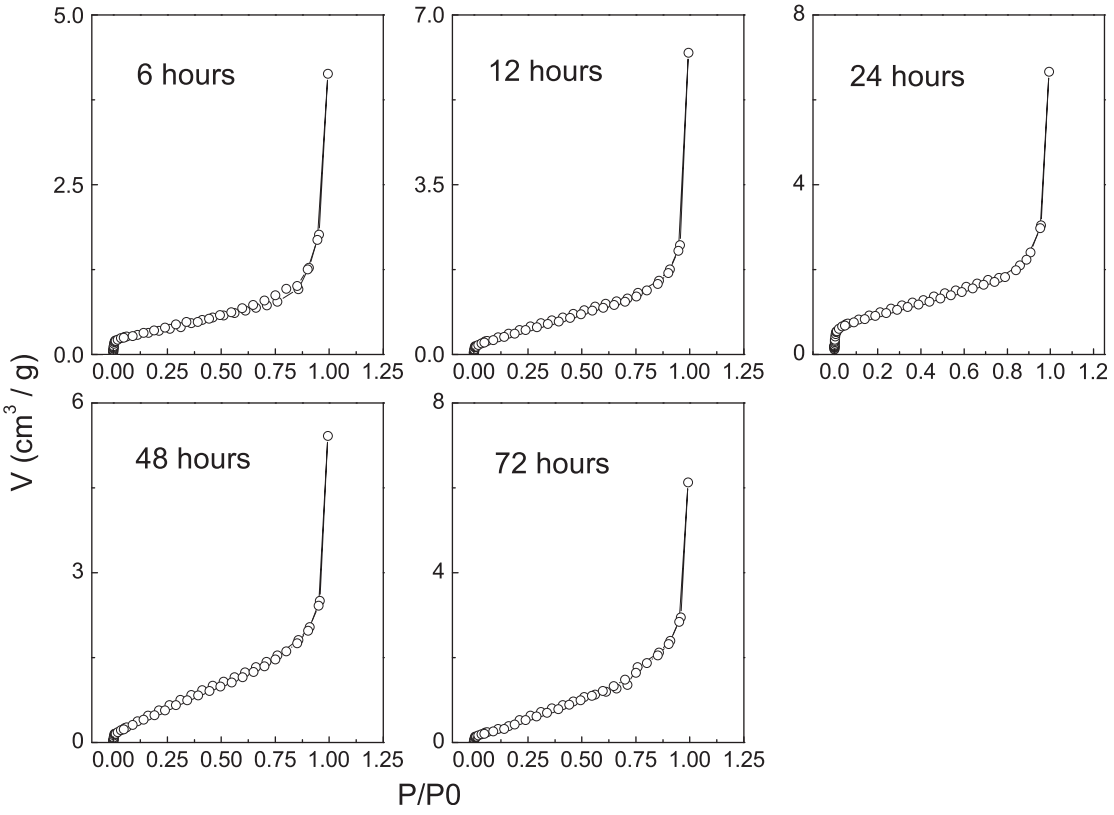

Fig. 2. Sorption curves as a function of the relative pressure.

the same data close to T_C. For all the samples the onset of the diamagnetic signal according to our experimental resolution starts at around the same critical temperature $T_C \approx 89 \pm 1$ K.

In Fig. 2 it is shown nitrogen adsorption/desorption isotherms for all the samples studied herein. The curves in the figure bring us with valuable information. All the curves are S-shaped isotherms classified as type-II according to the *International Union of Pure and Applied Chemistry* (*IUPAC*) classification representing multilayer adsorption in nonporous materials [21,22]. The knee located at low relatives pressures $P/P_0 \approx 10^{-2}$ indicates a monolayer formation of adsorbed N_2. These results are in agreement with previously reported ones for other *cuprates*, in particular for YBCO samples [26]. It should be noted that in all the curves there exist not hysteresis which means the no existence of capillarity condensation at large mesopores in the samples. The specific surface area (S_{BET}) values were obtained by following the multipoint Brunauer–Emmett–Teller (BET) analysis in the absorption region ($0.05 \leq P/P_0 \leq 0.3$), where the theory is in good concordance with the experimental data [22]. The experimental values were: 1.3 m^2/g, 2.2 m^2/g, 3.6 m^2/g, 2.7 m^2/g and 2.6 m^2/g for the samples with 6 h, 12 h, 24 h, 48 h and 72 h, respectively. These values are also of the same order of magnitude that the ones found for similar superconducting *cuprates*, including bulk YBCO [26].

One important characteristic of the pores is its distribution as a function of their sizes. Density functional theory (DFT) is a microscopic treatment of sorption phenomena that takes into account the presence of micropores and mesopores, which have their bases on statistical mechanics analysis. The sorption isotherms at 77 K were analyzed through the Quenched Solid Density Functional Theory (QSDFT) which incorporates the effects of surface roughness and heterogeneity [27]. Fig. 3 shows the pore-size distribution function as $dV/dR=f(R)$, where V is the pore volume and R is the pore width, obtained by the QSDFT method and for the region of pore widths below 12.5 nm. The curve for the 6 h sample (see Fig. 3) shows a broad distribution while the others distributions present some kind of peak below 5 nm. Note that the 24 h sample has a pore distribution shifted to lower pore-sizes with a peak around 1 nm. Taking into account the IUPAC pore classification the curves of Fig. 3 suggest that the samples have a structure of pores containing a small proportion of micropores with a large quantity of mesopores of different scales.

Other intrinsic parameter which is closely related to the pore distributions rather than the quantity of pores is the fractal dimension exponent (D). It captures the geometric topography of the surface of the particles given an idea about the homogeneities or regularities of the pores as also of the surface of the particles. The value=2 represents a planar surface and its increase from the reference value (=2) gives an idea of the heterogeneity of the pore structure. The D exponents calculated through the Frenkel–Halsey–Hill theory on the desorption isotherm

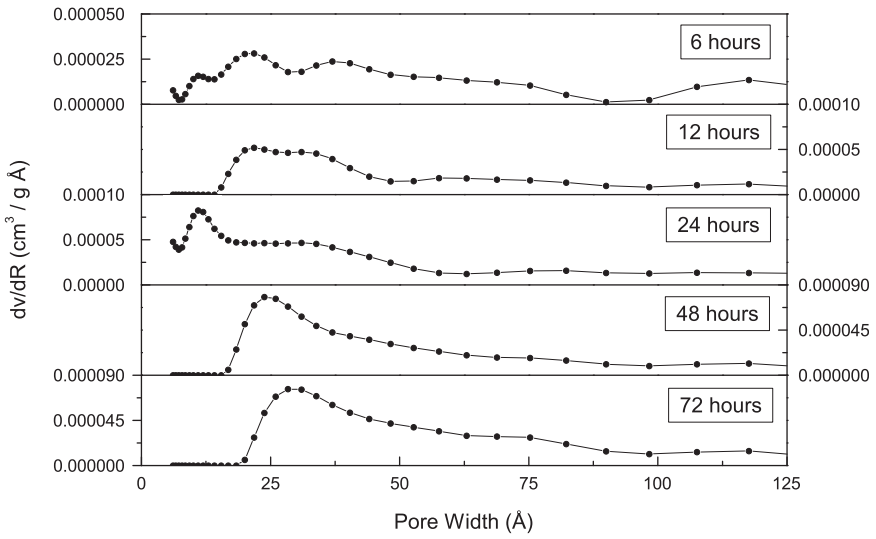

Fig. 3. Distribution of pore sizes $(dV/dR)=f(R)$ for all the samples.

Table 1
Features of the pore structure for the samples. Details are explained in the text.

Time h	S_{BET} m^2/g	V_T cm^3/g	V_{DR} cm^3/g	V_{micro} cm^3/g	V_{micro}/V_T %	r_P Å	D
6	1.3	6.4×10^{-3}	4.4×10^{-4}	5.4×10^{-4}	8	206	2.54
12	2.2	9.7×10^{-3}	4.2×10^{-4}	7.8×10^{-4}	8	177	2.51
24	3.6	1.0×10^{-2}	1.2×10^{-3}	1.6×10^{-3}	16	115	2.65
48	2.7	8.4×10^{-3}	4.1×10^{-4}	8.8×10^{-4}	10	125	2.52
72	2.6	9.5×10^{-3}	4.3×10^{-4}	8.3×10^{-4}	9	144	2.45

as provided by the equipment were 2.54 (6 h), 2.51 (12 h), 2.65 (24 h), 2.52 (48 h) and 2.45 (72 h).

The porosity, reported as the total pore volume in cm^3 per gram, gives an idea of the quantity of volume of a sample that is occupied by pores. To this end the total adsorbate volume should be measure at relative pressures as high as possible in order to include large pores. The measured values at $P/P_0 \cong 0.99$ were 6.4×10^{-3} cm^3/g (6 h), 9.7×10^{-3} cm^3/g (12 h), 1.0×10^{-2} cm^3/g (24 h), 8.4×10^{-3} cm^3/g (48 h) and 9.5×10^{-3} cm^3/g (72 h). On the other hand, the volume occupied only by micropores (microporosity) can be determined through the Dubinin Radushkevich theory (DR method). The intercept in the linear extrapolation of log (liquid adsorbate volume) vs. $\log^2(P/P_0)$ in the limit about $P/P_0 < 0.1$ provides the microporosity in cm^3/g. In spite of the basic adsorption mechanisms in micropores are controversial; the method allows doing a comparison between the microporosity of the samples. The values (in cm^3/g) were 4.4×10^{-4} (6 h), 4.2×10^{-4} (12 h), 1.2×10^{-3} (24 h), 4.1×10^{-4} (48 h) and 4.3×10^{-4} (72 h). Also, as an attempt to evaluate the microporosity level, it was measured the volume filled by pores with a diameter lower than 2 nm (criterion for micropores according to IUPAC) a parameter that we identified in the text as $V_{micro.}$ These values, as also the relation V_{micro}/V_T for all the samples are reported in Table 1.

All the results obtained for the pore structure in our measurements as described above are summarized in Table 1 below. S_{BET} is the specific surface area calculated from the BET method, V_T is the total pore volume (porosity) found at $P/P_0 \approx 0.99$, V_{DR} represents the microporosity obtained from the DR theory, V_{micro} is also the pore volume for pores with diameter lower than ≈ 2 nm (micropores), r_P is the average pore radius and D is the fractal coefficient. In the next paragraphs we discuss our results. As a first observation, the experimental data show that the porosity level (V_T) increases with the sintering time reaching a maximum value for 24 h, while further sintering time no longer raises the porosity which remains lower than the one found for 24 h (see Table 1). This time dependence for V_T is also reproduced qualitatively by the specific surface area (S_{BET}) as shown at the top of Fig. 4, and also by V_{micro} as seen in the medium graph. It should be noted that two specific factors can raise S_{BET}, specifically, a decrease in particle size and/or a generation of porosity. In spite of an increasing sintering time promotes large grains and that should decreases S_{BET}, the direct relation between S_{BET} and the porosity shown in our data suggests that the change of the S_{BET} with the sintering time is mainly controlled by the modification of the porosity.

Two mechanisms acting during the sintering process can influence the porosity and its structure. One mechanism is the coarsening of the particles, where the larger grains growth at expense of others of small sizes (increasing the porosity), while the other is associated with shrinkage of the compact, where the grains growth with the generation of grain boundaries and a decreasing in the porosity [28]. Both mechanisms are present during the sintering and competing between themselves. Our data (V_T and V_{micro} in Table 1) suggest that for sintering times up to 24 h the first mechanism can be more important leading to an increase in porosity, while as the time is increased even more, the

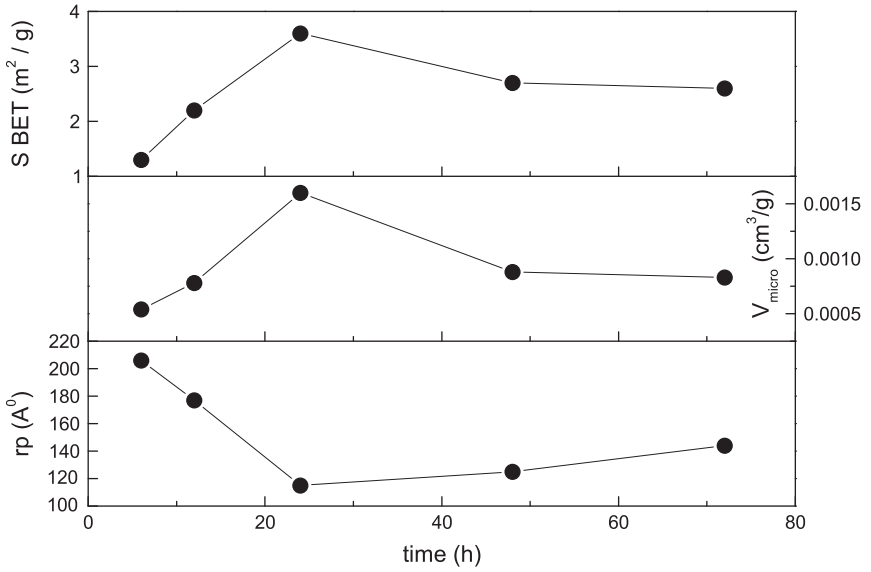

Fig. 4. Specific surface area of the particles (upper), volume occupied by micropores (medium), and average pore radius (lower) as a function of the sintering time. The solid line is a guide to the eyes.

large sizes of the preformed YBCO particles activate the second mechanism which dominates the process leading to a decreasing in the porosity.

In addition, another point to take into consideration is the diffusion of oxygen towards the interior of the samples during the oxygenation process, which was performed here at low temperatures (450 °C) and after the sintering. At high oxygen content the YBCO undergoes a tetragonal to orthorhombic (T–O) structural phase transformation which is crucial to the superconducting character of the samples. This phase transformation comes accomplish of anisotropic changes in the volume of the unit cell, and this results in a stress which is relaxed through the developing of microcracks in the samples [29]. During the oxygenation the pores formed through the sintering can be enhanced towards these cracks leading to an increase in the porosity level [29]. Since all the samples were oxygenated in identical conditions we cannot rule out this as another mechanism which can enhance the porosity in all the samples. Specifically, we can speculate that since the 24 h sample has a great quantity of pores before O_2 annealing, the own oxygenation process can enhance its porosity even more than the others samples.

It should be highlighted that the V_T parameter (i.e., the porosity level) takes into account all the empty spaces that there exist inside the samples, including micro, mesopores, macropores, and so on. Also we have used two methods to estimate the volume of pores belonging to the micropores class. The first is the DR theory which allows an indirect estimation of the microporosity volume (V_{DR}), while the second one is a direct measure of the volume for pores with diameter below 2 nm (V_{micro} in Table 1). Both dependences with the time $V_{DR}(t)$ and $V_{micro}(t)$ can be noted in Table 1. As can be seen the samples show an almost constant V_{DR} volume around $\approx 4.2 \times 10^{-4}$ cm^3/g, with the exception of the sample sintered during 24 h which has its microporosity significantly increased to 1.2×10^{-3} cm^3/g. The same qualitative behavior can be verified if the microporosity is analyzed through V_{micro}, as can be observed in the medium graph of Fig. 4. Also Table 1 shows a relative V_{micro}/V_T ratio between 8% and 10% for all the samples, except for the one sintered during 24 h where a significant increasing at around 16% can be seen. In general our results evidence that sintering during 24 h induces a change in the pore structure which is characterized by an accented development of micropores.

This last conclusion is in concordance with Fig. 3, where a closely inspection reveals that the curve for the 24 h sample is substantially shifted to the left as compared to the others. The increasing of the microporosity should be traduced in a decreasing of the average volume of the pores, and consequently, a lower average pore size. The experimental system allows calculating an average pore radius (r_P) of the pores and its dependence with the sintering time can be observed at the bottom graph of Fig. 4. The $r_P(t)$ dependence showed in Fig. 4 shows r_P with a minimum value at just 24 h, which is consistent with the generation of microporosity at this specific sintering time. In line with that the fractal coefficient of the samples is around $D \approx 2.5$, except for the sample sintered during 24 h where D slightly higher = 2.6. This slight high fractal coefficient in the 24 h sample reflects a more heterogeneous pore structure as a consequence of the generation of microporosity. We note that a broader pore distribution with pores of different scales leads to a more heterogeneous particle structure.

Finally we discuss briefly how some of our results can be relevant for the superconducting properties of bulk materials. The first important point is the high surface area and porosity of the sample sintered during 24 h. This can be crucial for the oxygenation process of bulk superconductors, since a higher surface area ensures an optimal contact of the oxygen with the external area of the particles, while the porosity helps in the O_2 diffusion to

the interior of the particles, providing a better oxygenation of the sample as a whole. As a second point we note that samples having a more disordered geometric topography of the surface of the particles (it means a higher fractal coefficient) should exhibit a higher possibility of having more contacts between their components (grains), which represent more ways for the current flow, promoting a higher current percolation along the macroscopic sample.

4. Conclusions

In summary, our results show that the sintering time has a strong influence on the pore structure for YBCO ceramic samples sintered at high temperatures as 950 °C. For all the samples the pore structure is formed majority by a large proportion of meso and macropores with a small quantity of micropores. The porosity and the specific surface area have a peak for the sample sintered during 24 h. The increasing of the porosity for this sample is mainly determined by the generation of micropores as verified in the experimental data. This leads to a sample (24 h) with a more heterogeneous pore structure if compared to the other ones which can be useful for the supercurrent transport in these ceramic materials. Our results show, from a quantitative and also quantitative point of view, how the sintering conditions in YBCO bulk superconductors influence the presence of pores and their principal features.

References

[1] J. Bock, F. Breuer, H. Walter, M. Noel, R. Kreutz, M. Kleinmaier, K.-H. Weck, S. Elschner, Development and successful testing of an MCP BSCCO-2212 components for a 10 MVA resistive superconducting fault current limiter, Superconductor Science and Technology 17 (2004) S122–S126.

[2] M. Tomita, M. Murakami, High-temperature superconductor bulk magnets that can trap magnetic fields of over 17 T at 29 K, Nature 421 (2003) 517–520.

[3] M. Miki, B. Felder, K. Tsuzuki, Z. Deng, N. Shinohara, M. Izumi, T. Ida, H. Hayakawa, Influence of AC magnetic field on a rotating machine with Gd-bulk HTS field-pole magnets, IEEE Transactions on Applied Superconductivity 21 (2011) 1185–1189.

[4] M. Strasik, J.R. Hull, J.A. Mittleider, J.F. Gonder, P.E. Johnson, K.E. McCrary, C.R. McIver, An overview of boeing flywheel energy storage systems with high-temperature superconducting bearings, Science and Technology 23 (2010) 034021.

[5] J.R. Hull, M. Murakami, Applications of bulk high-temperature superconductors, Proceedings of the IEEE 92 (2004) 1705–1718.

[6] M.F. Imayev, D.B. Kabirova, R.I. Sagito, K.A. Churbaeva, Relation between change of porosity and parameters of grains during annealing of the superconducting ceramics $YBa_2Cu_3O_{7-x}$, Journal of the European Ceramic Society 32 (2012) 1261–1268.

[7] E.S. Reddy, N.H. Babu, Y. Shi, D.A. Cardwell, G.J. Schmitz, Processing of large grain Y-123 superconductors with pre-defined porous structures, Superconductor Science and Technology 18 (2005) S15–S18.

[8] W.H. Tuan, T.A.O. Tien, Effect of addition of a small amount of silver on the microstructure and mechanical properties of $YBa_2Cu_2O_{7-x}$, Materials Chemistry and Physics 39 (1994) 72–75.

[9] M.J. Kramer, S.R. Arrasmith, Evaluation of techniques for fabricating very fine grained $YBa_2Cu_3O_{7-\delta}$+Ag composites, IEEE Transactions on Magnetics 27 (1991) 920–922.

[10] D.A. Cardwell, Processing and properties of large grain (RE)BCO, Materials Science and Engineering: B 53 (1998) 1–10.

[11] S. Umakosh, Y. Ikeda, A. Wongsatanawarid, C. Kim, M. Murakami, Top-seeded infiltration growth of Y–Ba–Cu–O bulk superconductors, Physica C 471 (2011) 843–845.

[12] A. Mahmood, Y.S. Chu, T.H. Sung, Enhancement of critical current density of liquid-infiltration-processed Y–Ba–Cu–O bulk superconductors using milled Y_2BaCuO_5 powder, Superconductor Science and Technology 25 (2012) 045008.

[13] K. Iida, N.H. Babu, Y. Shi, D.A. Cardwell, Seeded infiltration and growth of large, single domain Y–Ba–Cu–O bulk superconductors with very high critical current densities, Superconductor Science and Technology 18 (2005) 1421–1427.

[14] N.D. Kumar, T. Rajasekaran, V. Seshu Bai, YBCO/Ag composites through a preform optimized infiltration and growth process yield high current densities, Superconductor Science and Technology 24 (2011) 085005.

[15] H. Salamati, A.A. Babaei-Brozeny, M. Safa, Investigation of weak links and the role of silver addition on YBCO superconductors, Superconductor Science and Technology 14 (2001) 816–819.

[16] W.H. Tuan, J.M. Wu, Effect of microstructure on the hardness and fracture toughness of $YBa_2Cu_3O_{7-x}$/Ag composites, Journal of Materials Science 28 (1993) 1415–1420.

[17] T. Schuster, M.R. Koblischka, B. Ludescher, D.R. Henes, A. Kottmann, H. Kronmiiller, Variation of grain sizes in sintered $YBa_2Cu_3O_{7-\delta}$ by different sintering conditions, Materials Letters 14 (1992) 189–192.

[18] M. Kuwabara, H. Shimooka, Grain size dependence of the critical current density in $YBa_2Cu_3O_x$ superconductors, Applied Physics Letters 55 (1989) 2781–2783.

[19] S.R. Curras, J.A. Veira, J. Maza, F. Vidal, Critical current density versus normal-state resistivity in granular high-temperature superconductors with different average grain size, Superconductor Science and Technology 13 (2000) 1005–1010.

[20] M. Gervais, P. Odier, J.P. Coutures, Implications of the Y_2O_3–BaO–CuO liquidus for processing pure $YBa_2Cu_3O_{7-x}$ material, Materials Science and Engineering B 8 (1991) 287–294.

[21] F. Rouquerol, J. Rouquerol, K. Sing, Adsorption by powders & porous materials: principles, Methodology and Applications, Academic Press, 1999.

[22] S. Lowell, J.E. Shields, M.A.R. Thomas, M. Thomas, Characterization of Porous Solids and Powders: Surface Area, Pore Size and Density, Springer, 2004.

[23] P.K. Gallagher, Characterization of $Ba_2YCu_3O_x$ as a function of oxygen partial pressure 1. Thermoanalytical measurements, Advanced Ceramic Materials 2 (1987) 632–639.

[24] D.M. Kroeger, A. Choudhury, J. Brynestad, R.K. Williams, R.A. Padgett, W.A. Coghlan, Grain-boundary compositions in $YBa_2Cu_3O_{7-x}$ from Auger electron spectroscopy of fracture surfaces, Journal of Applied Physics 64 (1988) 331–335.

[25] P. Staszczuk, G.W. Chadzynski, D. Sternik, Thermogravimetric and microgravimetric studies of the surface properties of a high-temperature superconductor, Journal of Thermal Analysis and Calorimetry 62 (2000) 451–459.

[26] P. Staszczak, D. Stemick, G.W. Chadzyńsky, V.V. Kularov, Characterization of physicochemical properties of high-temperature superconductor surfaces using nitrogen adsorption, Journal of Alloys and Compounds 367 (2004) 277–282.

[27] A. Neimark, Y. Lin, P. Ravikovitch, M. Thommes, Quenched solid density functional theory and pore size analysis of micro-mesoporous carbons, Carbon 47 (2009) 1617–1628.

[28] M.W. Barsoun, Fundamentals of Ceramics, Institute of Physics Publishing, Bristol and Philadelphia, 2003.

[29] J.J. Roa, F.T. Dias, M. Matinez, J. Padilla, M. Segarra, Oxygenation kinetics of YBCO–TSMG samples using the nanoindentation technique, Journal of the European Ceramic Society 32 (2012) 425–431.